

Journal Pre-proofs

Biological evaluation and SAR analysis of novel covalent inhibitors against fructose-1,6-bisphosphatase

Xinya Han, Yunyuan Huang, Lin Wei, Haifeng Chen, Yanrong Guo, Zilong Tang, Wei Hu, Qinfei Xia, Qi Wang, Jufen Yan, Yanliang Ren

PII: S0968-0896(20)30454-5
DOI: <https://doi.org/10.1016/j.bmc.2020.115624>
Reference: BMC 115624

To appear in: *Bioorganic & Medicinal Chemistry*

Received Date: 27 March 2020
Revised Date: 12 June 2020
Accepted Date: 16 June 2020

Please cite this article as: Han, X., Huang, Y., Wei, L., Chen, H., Guo, Y., Tang, Z., Hu, W., Xia, Q., Wang, Q., Yan, J., Ren, Y., Biological evaluation and SAR analysis of novel covalent inhibitors against fructose-1,6-bisphosphatase, *Bioorganic & Medicinal Chemistry* (2020), doi: <https://doi.org/10.1016/j.bmc.2020.115624>

This is a PDF file of an article that has undergone enhancements after acceptance, such as the addition of a cover page and metadata, and formatting for readability, but it is not yet the definitive version of record. This version will undergo additional copyediting, typesetting and review before it is published in its final form, but we are providing this version to give early visibility of the article. Please note that, during the production process, errors may be discovered which could affect the content, and all legal disclaimers that apply to the journal pertain.

© 2020 Elsevier Ltd. All rights reserved.



Biological evaluation and SAR analysis of novel covalent inhibitors against fructose-1,6-bisphosphatase

Xinya Han^{1, #}, Yunyuan Huang^{2, #}, Lin Wei^{2, #}, Haifeng Chen³, Yanrong Guo¹, Zilong Tang⁴, Wei Hu¹, Qinfei Xia¹, Qi Wang¹, Jufen Yan^{1, *}, Yanliang Ren^{2, *}

¹School of Chemistry and Chemical Engineering, Anhui University of Technology, Maanshan 243002, China

²International Cooperation Base of Pesticide and Green Synthesis (Hubei), Key Laboratory of Pesticide & Chemical Biology (CCNU), Ministry of Education, Department of Chemistry, Central China Normal University, Wuhan 430079, China

³Ocean College, Beibu Gulf University, Qinzhou 535011, China

⁴Key Laboratory of Theoretical Chemistry and Molecular Simulation of Ministry of Education, Hunan University of Science and Technology, Xiangtan 411201, China

ABSTRACT

Fructose-1,6-bisphosphatase (FBPase) is an attractive target for affecting the GNG pathway. In our previous study, the C128 site of FBPase has been identified as a new allosteric site, where several nitrovinyl compounds can bind to inhibit FBPase activity. Herein, a series of **nitrostyrene** derivatives were further synthesized, and their inhibitory activities against FBPase were investigated *in vitro*. Most of the prepared nitrostyrene compounds exhibit potent FBPase inhibition ($IC_{50} < 10 \mu M$). Specifically, when the substituents of F, Cl, OCH₃, CF₃, OH, COOH, or 2-nitrovinyl were installed at the R₂ (meta-) position of the benzene ring, the FBPase inhibitory activities of the resulting compounds increased 4.5-55 folds compared to those compounds with the same groups at the R₁ (para-) position. In addition, the preferred substituents at the R₃ position were Cl or Br, thus compound **HS36** exhibited the most potent inhibitory activity ($IC_{50} = 0.15 \mu M$). The molecular docking and site-directed mutation suggest that C128 and N125 are essential for the binding of **HS36** and FBPase, which is consistent with the C128-N125-S123 allosteric inhibition mechanism. The reaction enthalpy calculations show that the order of the reactions of compounds with thiol groups at the R₃ position is Cl > H > CH₃. CoMSIA analysis is consistent with our proposed binding mode. The effect of compounds **HS12** and **HS36** on glucose production in primary mouse hepatocytes were further evaluated, showing that the inhibition was 71% and 41% at 100 μM , respectively.

KEYWORDS Fructose-1,6-bisphosphatase (FBPase), FBPase inhibitors, covalent inhibitors

1. Introduction

T2DM (type 2 diabetes mellitus) has been increasing worldwide as a comprehensive disease, and research interest is continuing to grow[1, 2]. The prominent features of T2DM are insulin resistance and hyperglycemia, which mostly come from endogenous glucose (EGP)[3]. Current antidiabetic drugs mainly focus on elevating insulin secretion and relieving insulin resistance[2, 4-7]. Metformin is the only available drug for the primary, albeit indirect, decrease in EGP, indicating that EGP is an attractive target for controlling blood glucose levels, and much research remains to be done in this field[8, 9]. Gluconeogenesis (GNG) is a major factor for EGP to generate glucose, and in this process, the substrates pyruvate and lactate can be converted glucose[10]. More importantly, the strategy of blocking the GNG pathway is considered a promising strategy for developing antidiabetic drugs, that can be used to control EGP[11, 12]. Glucose-6-phosphatase (G6Pase), fructose-1,6-bisphosphatase (FBPase) and phosphoenolpyruvate carboxykinase (PEPCK) are important enzymes and the primary targets for GNG. However, G6Pase and PEPCK are also involved in other metabolic pathways, while FBPase is not, thus, it is an attractive target for only affecting the GNG pathway[12, 13].

Human liver FBPase catalyzes the conversion of fructose-1,6-bisphosphate (FBP) as the substrate to fructose-6-phosphate (F6P) and phosphate, and it's one of the rate-limiting reactions of the GNG pathway[14]. The endogenous allosteric agents adenosine monophosphate (AMP) and fructose-2,6-bisphosphate (FDP) can synergistically inhibit FBPase[15]. AMP binds to a unique allosteric site and causes a conformational change from the active state (R) to an inactive state (T), whereas FDP

binds to the substrate site and competes with FBP[16, 17]. Recently, metformin has been demonstrated to indirectly inhibit FBPase and then affect GNG by elevating AMP levels[18]. On the other hand, FBPase is overexpressed in some diabetic models, and these facts highlight the importance of FBPase as a target for regulating blood glucose[11, 19]. Moreover, substantial efforts have been devoted to discover AMP site inhibitors against FBPase, and a wide variety of inhibitors have been reported in the literatures[11, 13, 20-32]. In addition, the AMP mimic **MB07803**, the most successful FBPase inhibitor, has been advanced to clinical trials[11, 33].

Covalent inhibitors have higher ligand efficiencies and longer binding times relative to noncovalent inhibitors[34, 35]. In the past decade, some covalent inhibitors, such as ibrutinib, osimertinib and acalabrutinib, have been approved by the FDA (United States Food and Drug Administration), initiating a new era for covalent inhibitors[36-38]. In our previous work[39], **nitrostyrene (HS1)** could covalently bind to the C128 of FBPase with an IC_{50} value of 3.5 μ M by fragment screening. In this work, we synthesized a series of **nitrostyrene** derivatives and explored their structure-activity relationships. Furthermore, the biological activities of the prepared compounds were evaluated in primary hepatocytes.

2. Results and discussion

2.1 Chemistry

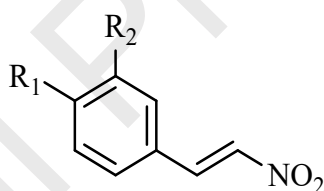
The synthetic route to target compounds was outlined in Scheme 1 and Scheme 2 in support information. All reagents were obtained from commercial suppliers and were used without further purification. TLC analysis were performed using precoated glass plates. Column chromatography separations were performed using silica gel (200–300

mesh). ^1H NMR and ^{13}C NMR spectra were obtained on Varian Mercury-Plus 400 and Varian NMR System 600 spectrometers. Chemical shifts are reported in ppm (δ) with the NMR solvent signals as an internal reference. Coupling constants (J) are reported in Hz. The abbreviations s, d, t and m refer to singlet, doublet, triplet and multiplet, respectively.

2.2 Nitrostyrene compounds against FBPase and structure-activity relationships.

In a previous work, phenyl groups have been shown to preferentially bind β -nitroalkenes over alkyl chains for inhibition activity[39]. Therefore, a benzene ring was selected as the scaffold for lead generation. Because a phenyl group linked to a β -nitroalkene (**HS1**) is a suitable structure for inhibiting FBPase, the side chain of this molecule would be the second moiety to be explored.

Table 1. Inhibitory activities of hit compounds (**HS1-HS22**) against FBPase.



Compound	R ₁	R ₂	Hu-FBPase IC ₅₀ (μM)
HS1	H	H	3.5 \pm 0.3
HS2	F	H	4.9 \pm 0.8
HS3	Cl	H	3.3 \pm 0.5
HS4	CH ₃	H	0.72 \pm 0.11
HS5	OCH ₃	H	16.0 \pm 1.8
HS6	SCH ₃	H	30.0 \pm 1.8
HS7	CF ₃	H	1.6 \pm 0.2
HS8	OH	H	15.0 \pm 1.6
HS9	COOH	H	25.0 \pm 1.8
HS10	NO ₂	H	0.49 \pm 0.07
HS11	CN	H	0.36 \pm 0.08
HS12	1,2,4-Triazole-1-yl	H	0.89 \pm 0.08

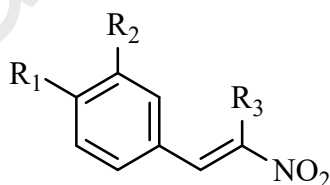
HS13	H	F	0.32 ± 0.02
HS14	H	Cl	0.34 ± 0.02
HS15	H	CH ₃	1.7 ± 0.3
HS16	H	OCH ₃	0.29 ± 0.03
HS17	H	CF ₃	0.40 ± 0.06
HS18	H	OH	0.24 ± 0.03
HS19	H	COOH	5.5 ± 0.3
HS20	H	NO ₂	1.7 ± 0.1
HS21	H	CN	0.38 ± 0.04
HS22	H	2-Nitrovinyl	0.38 ± 0.02

The SAR of substituent at the R₁ (para-) position of the benzene ring was explored using both electron-donating (e.g., CH₃, OCH₃, SCH₃, and OH) and electron-withdrawing (e.g., NO₂, CN, Cl, CF₃, and COOH) groups, and the results are summarized in **Table 1**. The addition of an electron-donating group, such as OH, OCH₃, or SCH₃, at the para-position of the benzene ring led to partial decrease in potency (**HS8**, **HS5**, and **HS6**, **Table 1**). These compounds had IC₅₀ values ranging from 15.0 to 30.0 μM, corresponding to a 4.3-8.5 folds decrease in potency relative to **HS1**. On the other hand, with the introduction of an electron-withdrawing group, such as Cl, CF₃, CN, and NO₂, at the para-position, the analogs showed similar or higher potencies than **HS1**. As shown in **Table 1**, significant improvements in potency were observed when NO₂, CN, or 1,2,4-triazole-1-yl was at the para-position. The substituted analogs displayed significantly higher potencies, the CN is most favorable (compound **HS11**, IC₅₀ = 0.36 μM), followed by NO₂ (compound **HS10**, IC₅₀ = 0.49 μM) and 1,2,4-triazole-1-yl group (compound **HS12**, IC₅₀ = 0.89 μM). The approximately 4 to 10-fold enhancement in potency over compound **HS1** suggested that the electron-withdrawing groups (CN, NO₂, or 1,2,4-triazole-1-yl) at the para-position of compound **HS1** is favorable for the

FBPase inhibitory activities. However, when a COOH was introduced, the compound **HS9** exhibited 7.1-fold decrease in potency in comparison with **HS1**, likely because the carboxyl group has remarkable solvation effect.

To further elucidate the effects of the position of the substituents on the benzene ring on inhibition, compounds **HS13-HS22** were synthesized, and the relative results were summarized in **Table 1**. Introducing the F, Cl, OCH₃, CF₃, OH, COOH or 2-nitrovinyl at the R₂ (meta-) position of the benzene ring, afforded analogs with IC₅₀ values of 0.29-5.5 μM, corresponding to 4.5-55 folds improvements over the analogs with substituents at the para-position. These results suggest that the F and Cl groups at the meta-position are preferred over the same groups at the para-position and suggest that substituents at the meta-position of the benzene ring play a key role in the binding interactions between FBPase and compounds of this series and can enhance their FBPase inhibitory potency.

Table 2. Inhibitory activities of hit compounds (**HS23-HS36**) against FBPase.



Compound	R ₁	R ₂	R ₃	Hu-FBPase IC ₅₀ (μM)
HS23	H	H	CH ₃	16.0 ± 2.5
HS24	CN	H	CH ₃	5.1 ± 0.4
HS25	H	H	Br	0.21 ± 0.04
HS26	H	H	Cl	0.16 ± 0.02
HS27	H	CN	Br	0.23 ± 0.02
HS28	CN	H	Br	0.27 ± 0.02
HS29	H	F	Br	0.23 ± 0.04
HS30	F	H	Br	0.64 ± 0.03

HS31	H	Cl	Cl	0.34 ± 0.04
HS32	Cl	H	Cl	0.54 ± 0.03
HS33	H	CN	Cl	0.21 ± 0.03
HS34	CN	H	Cl	0.30 ± 0.04
HS35	H	NO ₂	Cl	0.37 ± 0.03
HS36	NO ₂	H	Cl	0.15 ± 0.03

To further optimize the 2-nitrovinylbenzene scaffold, the introduction of substituents at the R₃ position was explored and the results were summarized in **Table 2**. The addition of a CH₃ group at the R₃ position (**HS23**, IC₅₀ = 16.0 μM) led to slight decrease in activity over compound **HS1**, while the introduction of a CH₃ group at the R₃ position of **HS11** (**HS24**, IC₅₀ = 5.1 μM) result in 14-fold decrease in potency relative to that of the parent compound. These results suggest that the introduction of a CH₃ group at the R₃ position is unsuitable for improving potency. However, adding Br or Cl group at the R₃ position of **HS1**, the corresponding compounds (**HS25** and **HS26**) showed 16.6-fold and 21.8-fold increases in potency, with the IC₅₀ values of 0.21 μM and 0.16 μM, respectively. This indicate that the chloro and bromo substituted analogs are more potent than analogs with CH₃ substituents and that the installation of a halogen substituent at the R₃ position is favorable for increasing potency. As in this case, having determined that CN, NO₂, F, Cl, and CH₃ are the preferred groups on the benzene ring, Br or Cl groups was introduced at the R₃ position of the corresponding compounds, and the FBPase inhibitory potencies of the resulting compounds were explored. As shown in **Table 2**, **HS27-HS36** were generally more potent than the analogs without Br or Cl groups at the R₃ position, the IC₅₀ values of them ranging from 0.15 to 0.72 μM. Among

all the tested compounds, **HS36** ($IC_{50} = 0.15 \mu M$) with a NO_2 group at the meta-position and a Br group at the R_3 position was the most potent compound.

2.3 The binding modes of compounds **HS1** and **HS36** against the C128 site of **FBPase**.

To explore the binding model in detail, compounds **HS1** and **HS36** were selected as probe molecules for studying the interactions with **FBPase** using the covalent docking module of Autodock. The possible binding modes of compounds **HS1** and

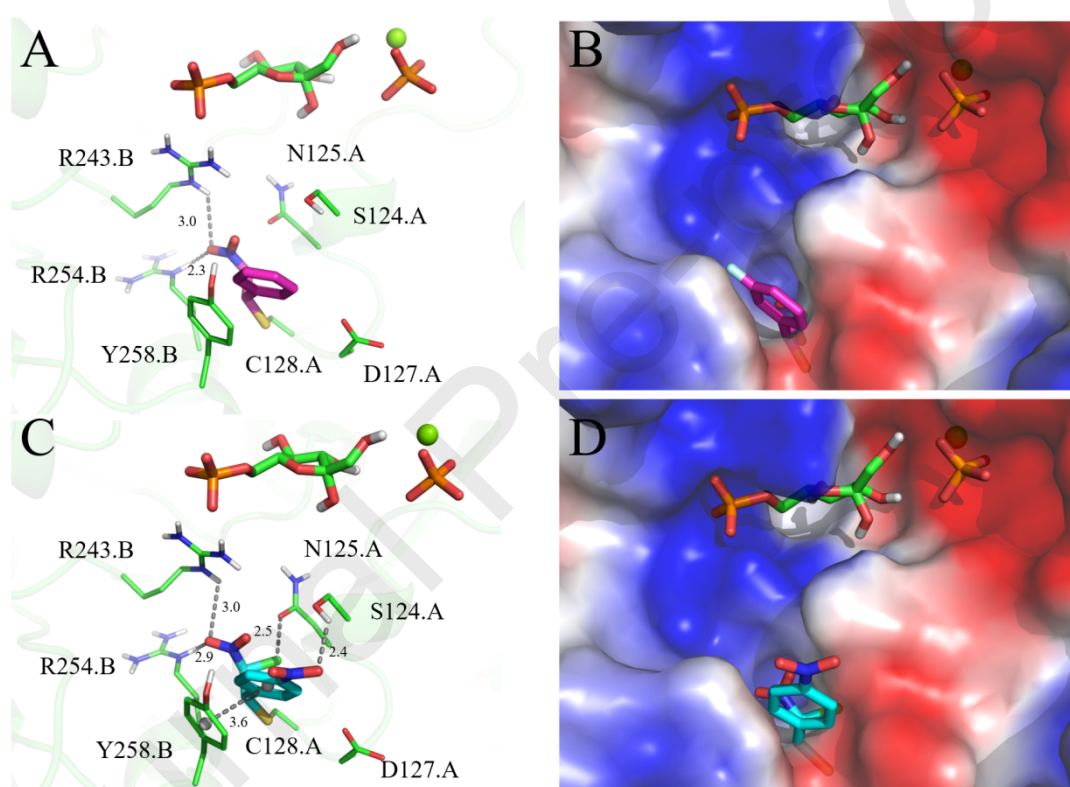


Figure 1. Reasonable binding modes of **HS1** (A) and **HS36** (C) into the C128 site of **FBPase** docked by Autodock. The binding models of **HS1** (B) and **HS36** (D) with the surface electrostatic potential.

HS36 are shown in **Figure 1**. However, compound **HS1** or **HS36** did not conflict with **F6P** and was located at the bottom of the substrate pocket. Obviously, a covalent bond was formed between SH of C128.A and the β carbon of compound **HS1** or **HS36**. The nitro group of compound **HS1** could form two hydrogen bonding interactions with the

NH₂ groups of R254.B and R243.B. In addition, the meta-substituent on **HS1** is close to the OH group of Y258.B. These results suggest that elevating the inhibitory activity of compound **HS13** compared with that of compound **HS1** relies on this hydrogen bonding interaction, and a substituent at the meta-position is better than one at the para-position for achieving this hydrogen bonding interaction. In addition, the NO₂ group of compound **HS36** could form two hydrogen bonding interactions with the NH₂ group of R254.B and R243.B. The nitro moiety at the meta-position on benzene in compound **HS36** could form a hydrogen bond with OH group of S124.A. The benzene ring of **HS36** can form π - π interaction with the phenyl ring of Y258.B.

Table 3. The IC₅₀ of **HS36** against FBPase mutations.

	WT	C128S	S124A	N125A	D127A	R243A	R254A	Y258A
Specific activity (U/mg)	4.0±0.2	2.7±0.2	5.0±0.2	2.7±0.2	1.5±0.1	2.5±0.3	1.9±0.1	3.5±0.2
HS36 IC ₅₀ (μM)	0.15±0.03	195±15	1.3±0.1	26.4±3.1	0.56±0.10	1.4±0.1	2.2±0.2	0.91±0.12
HS36 (IC ₅₀ ^M /IC ₅₀ ^W)	1	1300	8.7	176	3.7	9.3	14.7	6.1

To identify the interactions of **HS36** and FBPase, the C128, S124, N125, D127, R243, R254 and Y258 were mutated to Ser or Ala. As listed in **Table 3**, C128S and N125A substitutions led to 1300-fold (195 μM) and 176-fold (26.4 μM) increases in the IC₅₀ values compared with those for wild-type FBPase (0.15 μM). These experimental results suggest that C128 and N125 are of great importance for binding of compound **HS36** and FBPase, which is consistent with our previously reported binding model and the C128-N125-S123 allosteric inhibition mechanism[39]. In comparison, the IC₅₀ values of S124A (1.3 μM), R243A (1.4 μM), R254A (2.2 μM) and Y258A (0.91 μM) are 8.7-fold, 9.3-fold 14.7-fold and 6.1-fold higher, respectively,

than that of wild-type FBPase, indicating that interactions between S124, R243, R254, Y258 and **HS36** exist.

Furthermore, the compounds with a halogen at the R₃ position displayed potent inhibitory activities against FBPase, but the compounds with CH₃ at R₃ showed lower activities. To elucidate the differences in the biological activity of these compounds, the effects of different substituents at R₃ on the reaction enthalpy were explored. All local minima in water were located by geometry optimization. The level of theory was ω B97xD/6-311++G**, and the solvation model was SMD. All quantum chemistry calculations were performed with the Gaussian 09 package. The reaction enthalpy is -18.65 kcal/mol for **HS1**, -18.24 kcal/mol for **HS23** and -20.83 kcal/mol for **HS26**. Thus, the order of the reactions of compounds with thiol groups at R₃ is Cl (**HS26**) > H (**HS1**) > CH₃ (**HS23**).

2.4 CoMSIA Analysis.

Comparative Molecular Similarity Index Analysis (CoMSIA) method is an effective tool for 3D-QSAR analysis. The PLS analysis results for the CoMSIA model are summarized in **Table 4**. A predictive CoMSIA model with a leave-one-out cross-validated coefficient (q^2) of 0.489 and a correlation coefficient (R^2) of 0.885 was built. As shown in **Figure 2**, the predicted activity values are in good agreement with the experimental data. The standard error ($S = 0.246$) and F-test value ($F = 52.102$) further corroborate the predicted model. In the QSAR model, the contributions of the steric and electrostatic fields are 9.5% and 90.5%, respectively.

Table 4. Statistical parameters of the CoMSIA Model

q^2	R^2	S	F	contribution (%)	
				steric	electrostatic
0.489	0.885	0.246	52.102	9.5	90.5

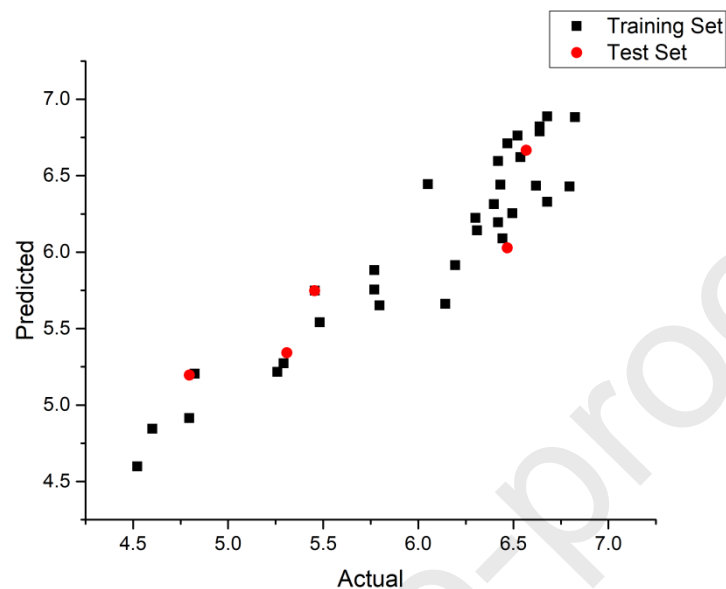


Figure 2. Plot of predicted vs experimental values for the training and test sets based on the CoMSIA model.

The CoMSIA contour maps shown in **Figure 3** present the steric and electrostatic fields. In the steric field map, the green contour surrounding the benzene ring suggests that more bulky substituents in these positions would be favorable for higher activity, while the yellow contour indicates the region of unfavorable steric effects. These results are consistent with our binding mode proposed above. In the CoMSIA electrostatic field, the blue region indicates that a negative charge may be favorable for inhibitory activity, whereas a positive charge is unfavorable.

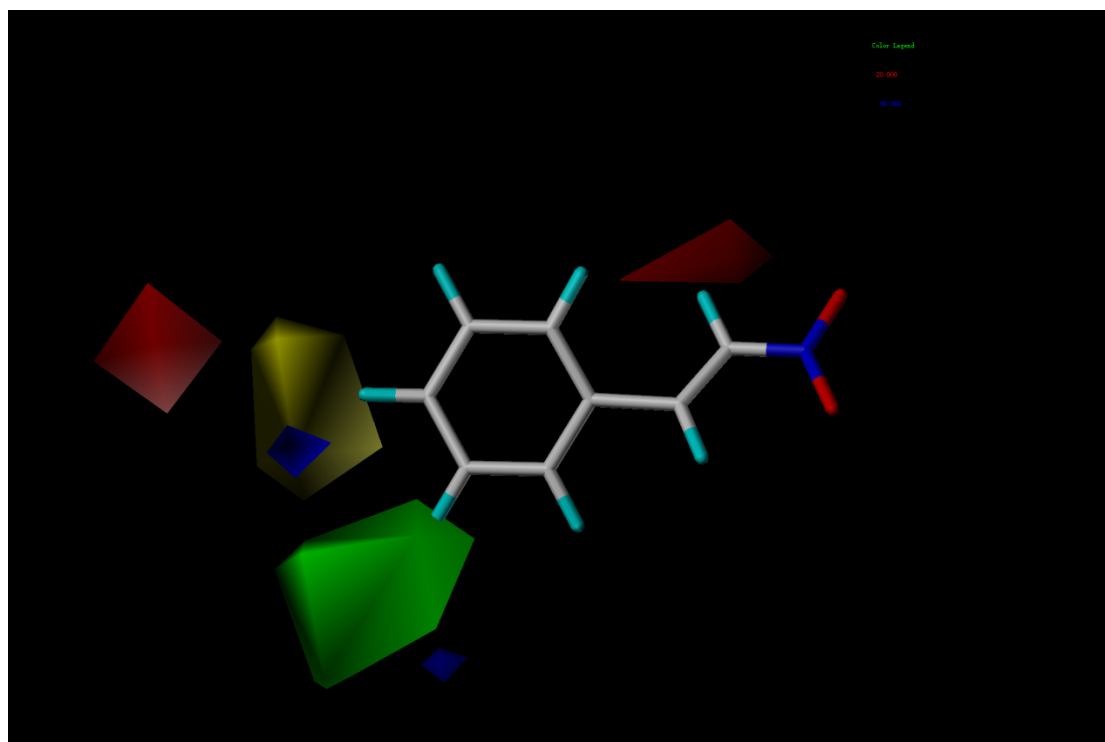


Figure 3. Steric and electrostatic maps of the CoMSIA model. **HS1** is shown inside the field. In the steric field contour plot, sterically favored areas are represented by green polyhedra, while sterically disfavored areas are represented by yellow polyhedra. In the electrostatic field contour plot, positive-charge-favored areas are represented by red polyhedra, whereas negative-charge-favored areas are represented by blue polyhedra.

2.5 Inhibition of Glucose Production in Hepatocytes.

As FBPase plays a central role in GNG, the nitrostyrene compounds were further evaluated based on glucose production in freshly isolated primary mouse hepatocytes. As illustrated in **Figure 4**, the representative nitrostyrene compounds (**HS12** and **HS36**) at 100 μM both effectively inhibited glucose production by primary mouse hepatocytes with lactate/pyruvate as the GNG substrate, compared with the 0.1% DMSO control group. **HS12** and **HS36** at 100 μM inhibited glucose production by approximately 71% and 41%, respectively. Metformin is as the only marketed drug recognized to acts, at

least partially, through the inhibition of GNG[12]. As a positive control, the inhibitory ability of metformin to glucose production by mouse hepatocytes was also evaluated[32].

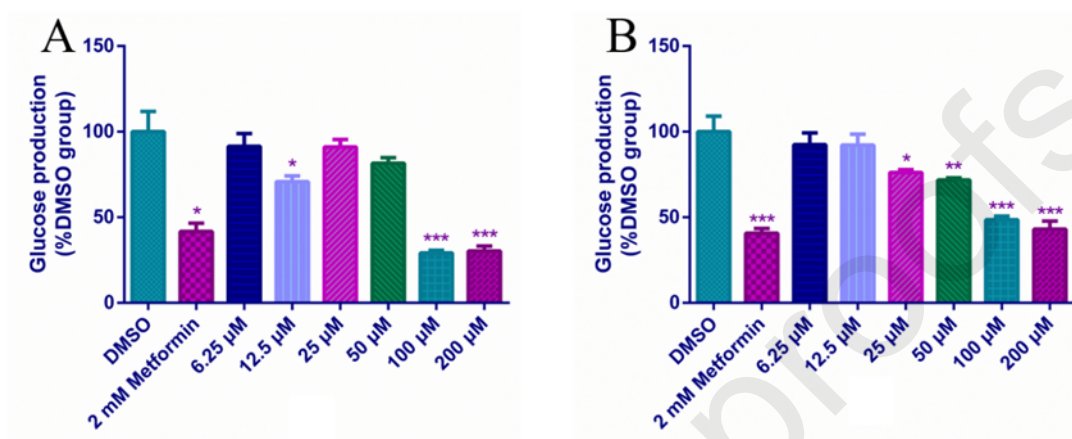


Figure 4. The compounds **HS12**(A), **HS36**(B), inhibition GNG assay on the primary mouse hepatocytes. Metformin (2 mM) was utilized as the control. *P < 0.05, **P < 0.01, ***P < 0.001 versus DMSO group.

3 Conclusion

In summary, a series of nitrostyrene derivatives were synthesized, and their inhibitory activities against FBPase were investigated *in vitro*. Most of the prepared nitrostyrene compounds could potentially inhibit (<10 μM) FBPase. Specifically, when the F, Cl, OCH₃, CF₃, OH, COOH, or 2-nitrovinyl substituents were installed at the meta-position, the FBPase inhibition activities of the resulting compounds increased 4.5-55 folds compared with those of the compound with the same group at the para-position. Moreover, the preferred substituents at the R₃ position were Cl or Br over CH₃ for increasing the inhibitory activity, and compound **HS36** exhibited the most potent inhibitory activity (IC₅₀ = 0.15 μM). The structure-activity relationship (SAR) has been

analyzed by the joint use of the reaction enthalpy calculations, molecular docking, site-directed mutagenesis and CoMSIA strategies. Subsequently, **HS36** can reduce glucose production in hepatocytes. In conclusion, this work can provide a new platform for designing covalent inhibitors of FBPase for treating T2DM. Further structural optimization of nitrostyrene compounds and the QSAR studies are well underway in our group.

4 Experimental

4.1 General methods

4.1.1. General procedure for the preparation of substituted 2-nitrovinyl benzene derivatives

An aromatic aldehyde (5 mmol) was dropped into a solution of ammonium acetate (12 mmol) in dry nitromethane (10 mL) and acetic acid (20 mL) at 90 °C with stirring. The mixture was then refluxed for 5 h, and the mixture was poured into water and extracted with ethyl acetate (3 × 50 mL). The extracts were washed with saturated saline solution, dried over Na₂SO₄, filtered and concentrated under reduced pressure. The residue was recrystallized from methanol or purified by column chromatography on silica gel (ethyl acetate / petroleum ether) to obtain the target 2-nitrovinyl benzene derivative.

4.1.2 General procedure for the preparation of substituted 2-bromo-2-nitrovinyl benzene derivatives

To a stirred solution of a substituted 2-nitrovinyl benzene (10.0 mmol) in sodium acetate (12.0 mmol) in chloroform (10 mL) was dropwise added neat Br₂ (12.0 mmol) over 5 min at 0 °C. The cloudy yellow reaction mixture was then heated to reflux and stirred for 5-8 h (monitored by TLC). The excess Br₂ was removed by washing the reaction mixture with a saturated aqueous solution of Na₂S₂O₃. The aqueous solution was then extracted with CH₂Cl₂ (3 × 20 mL). The combined CH₂Cl₂ layers were dried over anhydrous Na₂SO₄. The solvent was removed by evaporation under reduced

pressure to give a crude solid that was purified by silica gel column chromatography using ethyl acetate and petroleum ether as the eluent.

4.1.3 General procedure for the preparation of substituted 2-chloro-2-nitrovinyl benzene derivatives

To a solution of substituted 2-nitrovinyl benzene (0.4 mmol) in wet DMF (2.7 mL, 0.15 M) was added iodobenzene dichloride (PhICl₂) (1.5 equiv) with stirring. The resulting mixture was maintained at room temperature, and the reaction progress was monitored by TLC. Upon completion, the reaction mixture was poured into cold water (30 mL) and extracted with CH₂Cl₂ (3 × 20 mL). The combined organic layers were washed with saturated NaHCO₃ (1 × 50 mL) and brine (1 × 50 mL) before being dried over anhydrous Na₂SO₄. The solvent was removed under vacuum and the residue was purified by silica gel chromatography, using a mixture of ethyl acetate and petroleum ether to afford the desired product.

(E)-(2-nitrovinyl) benzene (HS1)

Yield 88%. Yellow solid. M.p.: 57 – 58 °C. ¹H NMR (400 MHz, CDCl₃) δ: 8.01 (d, *J* = 13.7 Hz, 1H), 7.59 (d, *J* = 13.7 Hz, 1H), 7.55 (d, *J* = 7.1 Hz, 2H), 7.50 (d, *J* = 7.0 Hz, 1H), 7.48 – 7.42 (m, 2H). ¹³C NMR (101 MHz, CDCl₃) δ: 133.8, 131.9, 126.9, 124.89, 124.2, 123.9. MS (EI) *m/z*: 149.1 [M]⁺.

(E)-1-fluoro-4-(2-nitrovinyl) benzene (HS2)

Yield 78%. Yellow solid. M.p.: 100 – 101 °C. ¹H NMR (400 MHz, CDCl₃) δ: 7.98 (d, 1H), 7.65 – 7.49 (m, 3H), 7.20 – 7.06 (m, 4H). ¹³C NMR (101 MHz, CDCl₃) δ: 166.3, 163.8, 137.9, 137.0, 131.4, 131.4, 126.4, 117.0, 116.7. MS (EI) *m/z*: 167.2 [M]⁺.

(E)-1-chloro-4-(2-nitrovinyl) benzene (HS3)

Yield 77%. Yellow solid. M.p.: 113 – 114 °C. ¹H NMR (400 MHz, CDCl₃) δ: 7.96 (d, *J* = 13.9 Hz, 1H), 7.57 (dd, *J* = 13.7 Hz, 1H), 7.53 – 7.35 (m, 4H). ¹³C NMR (101 MHz, CDCl₃) δ: 138.4, 137.8, 137.6, 130.4, 129.9, 128.7. MS (EI) *m/z*: 183.1 [M]⁺.

(E)-1-methyl-4-(2-nitrovinyl) benzene (HS4)

Yield 88%. Yellow solid. M.p.: 101 – 103 °C. ¹H NMR (400 MHz, CDCl₃) δ: 7.97 (d, *J* = 13.7 Hz, 1H), 7.56 (d, *J* = 13.7 Hz, 1H), 7.44 (d, *J* = 7.7 Hz, 2H), 7.25 (d, *J* = 7.6 Hz, 2H), 2.40 (s, 3H). ¹³C NMR (101 MHz, CDCl₃) δ: 143.1, 139.1, 136.1, 130.1, 129.1, 127.2, 21.6. MS (EI) *m/z*: 163.2 [M]⁺.

(E)-1-methoxy-4-(2-nitrovinyl) benzene (HS5)

Yield 85%. Yellow solid. M.p.: 87 – 88 °C. ¹H NMR (400 MHz, CDCl₃) δ: 7.97 (d, *J* = 13.6 Hz, 1H), 7.55 – 7.46 (m, 3H), 6.96 (d, *J* = 8.8 Hz, 2H), 3.87 (s, 3H). ¹³C NMR (101 MHz, CDCl₃) δ: 162.9, 139.0, 134.9, 131.2, 122.5, 114.9, 77.4, 77.1, 76.8, 55.5. MS (EI) *m/z*: 179.1 [M]⁺.

(E)-methyl(4-(2-nitrovinyl) phenyl) sulfane (HS6)

Yield 80%. Yellow solid. M.p.: 84 – 86 °C. ¹H NMR (400 MHz, CDCl₃) δ: 7.94 (d, *J* = 13.6 Hz, 1H), 7.56 (d, *J* = 13.6 Hz, 1H), 7.44 (d, *J* = 8.4 Hz, 2H), 7.25 (d, *J* = 8.4 Hz, 2H), 2.51 (s, 3H). ¹³C NMR (101 MHz, CDCl₃) δ: 145.1, 138.7, 136.0, 129.4, 126.10, 125.9, 14.8. MS (EI) *m/z*: 195.2 [M]⁺.

(E)-1-(2-nitrovinyl)-4-(trifluoromethyl) benzene (HS7)

Yield 67%. Yellow solid. M.p.: 90 – 92 °C. ¹H NMR (600 MHz, CDCl₃) δ: 8.03 (d, *J* = 13.7 Hz, 1H), 7.73 (d, *J* = 8.2 Hz, 2H), 7.68 (d, *J* = 8.1 Hz, 2H), 7.62 (d, *J* = 13.7 Hz, 1H). ¹³C NMR (151 MHz, CDCl₃) δ: 138.8, 137.1, 133.4, 129.3, 126.3. MS (EI) *m/z*: 217.2 [M]⁺.

(E)-4-(2-nitrovinyl) phenol (HS8)

Yield 69%. Yellow solid. M.p.: 163 – 165 °C. ¹H NMR (600 MHz, DMSO-*d*₆) δ: 10.45 (s, 1H), 8.07 (s, 2H), 7.73 (d, *J* = 8.5 Hz, 2H), 6.87 (d, *J* = 8.5 Hz, 2H). ¹³C NMR (151 MHz, DMSO-*d*₆) δ: 162.0, 140.3, 135.2, 132.8, 121.5, 116.6. MS (EI) *m/z*: 165.2 [M]⁺.

(E)-4-(2-nitrovinyl) benzoic acid (HS9)

Yield 79%. Yellow solid. M.p.: > 250 °C. ¹H NMR (600 MHz, DMSO-*d*₆) δ: 13.38 (s, 1H), 8.32 (d, *J* = 13.6 Hz, 1H), 8.20 (d, *J* = 13.6 Hz, 1H), 8.03 (d, *J* = 8.1 Hz, 2H), 7.98 (d, *J* = 8.2 Hz, 2H). ¹³C NMR (151 MHz, DMSO-*d*₆) δ: 167.1, 139.9, 138.3, 134.6, 134.3, 130.2, 130.2. MS (EI) *m/z*: 193.1 [M]⁺.

(E)-1-nitro-4-(2-nitrovinyl) benzene (HS10)

Yield 79%. Yellow solid. M.p.: 201 – 202 °C. ¹H NMR (600 MHz, CDCl₃) δ: 8.33 (d, *J* = 8.6 Hz, 2H), 8.05 (d, *J* = 13.7 Hz, 1H), 7.74 (d, *J* = 8.6 Hz, 2H), 7.65 (d, *J* = 13.7 Hz, 1H). ¹³C NMR (151 MHz, Acetone-*d*₆) δ: 140.6, 136.9, 136.1, 130.5, 124.1. MS (EI) *m/z*: 194.1 [M]⁺.

(E)-4-(2-nitrovinyl) benzonitrile (HS11)

Yield 75%. Yellow solid. M.p.: 184 – 185 °C. ¹H NMR (600 MHz, CDCl₃) δ: 8.00 (d, *J* = 13.7 Hz, 1H), 7.77 (d, *J* = 8.3 Hz, 2H), 7.67 (d, *J* = 8.3 Hz, 2H), 7.63 (d, *J* = 13.8 Hz, 1H). ¹³C NMR (151 MHz, CDCl₃) δ: 139.4, 136.6, 134.3, 133.0, 129.4, 117.8, 115.2. MS (EI) *m/z*: 174.0 [M]⁺.

(E)-1-(4-(2-nitrovinyl) phenyl)-1H-1,2,4-triazole (HS12)

Yield 65%. Yellow solid. M.p.: > 200 °C. ¹H NMR (600 MHz, DMSO-*d*₆) δ: 9.45 (s, 1H), 8.33 (d, *J* = 14.0 Hz, 2H), 8.20 (d, *J* = 13.6 Hz, 1H), 8.09 (d, *J* = 8.7 Hz, 2H), 8.01 (d, *J* = 8.7 Hz, 2H). ¹³C NMR (101 MHz, DMSO-*d*₆) δ: 157.7, 147.7, 143.8, 143.3, 143.0, 136.4, 134.5, 124.5. MS (EI) *m/z*: 216.1 [M]⁺.

(E)-1-fluoro-3-(2-nitrovinyl) benzene (HS13)

Yield 72%. Yellow solid. M.p.: 45 – 47 °C. ¹H NMR (600 MHz, CDCl₃) δ: 7.97 (d, *J* = 13.6 Hz, 1H), 7.57 (d, *J* = 13.7 Hz, 1H), 7.45 (q, *J* = 7.5 Hz, 1H), 7.35 (d, *J* = 7.7 Hz, 1H), 7.25 (d, *J* = 9.2 Hz, 1H), 7.21 (t, *J* = 8.2 Hz, 1H). ¹³C NMR (151 MHz, CDCl₃) δ: 163.8, 162.1, 138.1, 137.7, 132.1, 132.1, 131.1, 131.1, 125.2, 119.1, 119.0, 115.5, 115.3. MS (EI) *m/z*: 167.0 [M]⁺.

(E)-1-chloro-3-(2-nitrovinyl) benzene (HS14)

Yield 77%. Yellow solid. M.p.: 47 – 48 °C. ¹H NMR (600 MHz, CDCl₃) δ: 7.98 – 7.90 (m, 1H), 7.59 (d, *J* = 13.8 Hz, 1H), 7.55 (s, 1H), 7.51 – 7.44 (m, 2H), 7.44 – 7.39 (m, 1H). ¹³C NMR (151 MHz, CDCl₃) δ: 138.0, 137.5, 135.3, 132.0, 131.8, 130.6, 128.7, 127.3. MS (EI) *m/z*: 183.3 [M]⁺.

(E)-1-methyl-3-(2-nitrovinyl) benzene (HS15)

Yield 81%. Yellow liquid. ¹H NMR (600 MHz, CDCl₃) δ 7.97 (d, *J* = 13.7 Hz, 1H), 7.58 (d, *J* = 13.7 Hz, 1H), 7.37 – 7.29 (m, 4H), 2.40 (s, 3H). ¹³C NMR (151 MHz, CDCl₃) δ: 134.1, 134.1, 131.7, 127.9, 124.8, 124.6, 124.1, 121.2, 16.1. MS (EI) *m/z*: 163.1 [M]⁺.

(E)-1-methoxy-3-(2-nitrovinyl) benzene (HS16)

Yield 77%. Yellow solid. M.p.: 91 – 93 °C. ¹H NMR (600 MHz, CDCl₃) δ: 7.97 (d, *J* = 13.6 Hz, 1H), 7.57 (d, *J* = 13.6 Hz, 1H), 7.37 (t, *J* = 8.2 Hz, 1H), 7.14 (d, *J* = 7.6 Hz, 1H), 7.04 (d, *J* = 6.5 Hz, 2H), 3.85 (s, 3H). ¹³C NMR (151 MHz, CDCl₃) δ: 154.9, 133.9, 132.1, 126.1, 125.3, 116.6, 112.8, 108.8, 50.3. MS (EI) *m/z*: 179.1 [M]⁺.

(E)-1-(2-nitrovinyl)-3-(trifluoromethyl) benzene (HS17)

Yield 69%. Yellow solid. M.p.: 75 – 76 °C. ¹H NMR (600 MHz, CDCl₃) δ: 8.04 (d, *J* = 13.7 Hz, 1H), 7.81 (s, 1H), 7.76 (d, *J* = 7.9 Hz, 2H), 7.65 (d, *J* = 13.6 Hz, 1H), 7.62 (d, *J* = 7.8 Hz, 1H). ¹³C NMR (151 MHz, CDCl₃) δ: 138.4, 137.3, 132.0, 131.8, 130.8, 130.0, 128.4, 125.7, 124.3, 122.5. MS (EI) *m/z*: 216.9 [M]⁺.

(E)-3-(2-nitrovinyl) phenol (HS18)

Yield 85%. Yellow solid. M.p.: 135 – 136 °C. ¹H NMR (600 MHz, CDCl₃) δ: 7.95 (d, *J* = 13.7 Hz, 1H), 7.56 (d, *J* = 13.6 Hz, 1H), 7.33 (t, *J* = 7.9 Hz, 1H), 7.13 (d, *J* = 7.6 Hz, 1H), 7.02 (s, 1H), 6.98 (d, *J* = 8.1 Hz, 1H). ¹³C NMR (151 MHz, DMSO-*d*₆) δ: 158.1, 139.8, 138.2, 131.8, 130.5, 121.0, 119.6, 116.5. MS (EI) *m/z*: 115.1 [M]⁺.

(E)-3-(2-nitrovinyl) benzoic acid (HS19)

Yield 85%. Yellow solid. M.p.: 194 – 195 °C. ¹H NMR (600 MHz, CDCl₃) δ: 8.30 (s, 1H), 8.23 (d, *J* = 7.8 Hz, 1H), 8.07 (d, *J* = 13.7 Hz, 1H), 7.80 (d, *J* = 7.7 Hz, 1H), 7.68 (d, *J* = 13.7 Hz, 1H), 7.61 (t, *J* = 7.7 Hz, 1H). ¹³C NMR (151 MHz, DMSO-*d*₆) δ: 166.8, 139.1, 138.5, 133.4, 132.6, 132.1, 131.0, 129.7. MS (EI) *m/z*: 193.2 [M]⁺.

(E)-1-nitro-3-(2-nitrovinyl) benzene (HS20)

Yield 75%. Yellow solid. M.p.: 122 – 123 °C. ¹H NMR (600 MHz, CDCl₃) δ: 8.43 (s, 1H), 8.36 (d, *J* = 8.2 Hz, 1H), 8.07 (d, *J* = 13.8 Hz, 1H), 7.89 (d, *J* = 7.6 Hz, 1H), 7.73 – 7.65 (m, 2H). ¹³C NMR (101 MHz, DMSO-*d*₆) δ: 153.2, 145.1, 141.8, 140.4, 137.2, 135.5, 130.9, 129.4. MS (EI) *m/z*: 194.1 [M]⁺.

(E)-3-(2-nitrovinyl) benzonitrile (HS21)

Yield 82%. Yellow solid. M.p.: 201 – 202 °C. ¹H NMR (600 MHz, Chloroform-*d*) δ: 7.99 (d, *J* = 13.7 Hz, 1H), 7.85 (s, 1H), 7.79 (d, *J* = 7.8 Hz, 2H), 7.64 – 7.60 (m, 2H). ¹³C NMR (151 MHz, cdcl₃) δ: 138.9, 136.4, 134.9, 132.7, 132.3, 131.4, 130.4, 117.5, 114.0. MS (EI) *m/z*: 174.1 [M]⁺.

1,3-bis((E)-2-nitrovinyl) benzene (HS22)

Yield 78%. Yellow solid. M.p.: 203 – 204 °C. ¹H NMR (400 MHz, CDCl₃) δ: 8.02 (d, *J* = 13.7 Hz, 2H), 7.69 (d, *J* = 8.0 Hz, 3H), 7.63 (d, *J* = 13.7 Hz, 2H), 7.60 – 7.55 (m, 1H). ¹³C NMR (101 MHz, DMSO-*d*₆) δ: 143.9, 143.0, 138.4, 136.2, 135.0, 134.2.

(E)-4-(2-nitroprop-1-en-1-yl) benzonitrile (HS24)

Yield 70%. Yellow solid. M.p.: 108 – 110 °C. ¹H NMR (600 MHz, CDCl₃) δ: 8.07 (s, 1H), 7.78 (d, *J* = 8.2 Hz, 2H), 7.56 (d, *J* = 8.1 Hz, 2H), 2.46 (s, 3H). ¹³C NMR (151 MHz, CDCl₃) δ: 149.6, 136.7, 132.3, 131.0, 130.0, 117.9, 112.9, 13.8. MS (EI) *m/z*: 188.1 [M]⁺.

(Z)-(2-bromo-2-nitrovinyl) benzene (HS25)

Yield 87%. Yellow solid. M.p.: 63 – 64 °C. ^1H NMR (600 MHz, CDCl_3) δ : 8.65 (s, 1H), 7.90 (d, $J = 7.1$ Hz, 2H), 7.56 – 7.48 (m, 3H). ^{13}C NMR (151 MHz, CDCl_3) δ : 136.4, 131.9, 130.9, 130.1, 128.9, 127.9. MS (EI) m/z : 226.9 $[\text{M}-1]^+$, 228.9 $[\text{M}+1]^+$.

(Z)-(2-chloro-2-nitrovinyl) benzene (**HS26**)

Yield 78%. Yellow solid. M.p.: 43 – 44 °C. ^1H NMR (600 MHz, CDCl_3) δ : 8.38 (s, 1H), 7.88 – 7.83 (m, 2H), 7.55 – 7.48 (m, 3H). ^{13}C NMR (151 MHz, $\text{DMSO}-d_6$) δ : 137.1, 132.5, 132.4, 131.6, 129.9, 129.4. MS (EI) m/z : 183.0 $[\text{M}]^+$.

(Z)-3-(2-bromo-2-nitrovinyl) benzonitrile (**HS27**)

Yield 65%. Yellow solid. M.p.: 92 – 93 °C. ^1H NMR (600 MHz, CDCl_3) δ : 8.60 (s, 1H), 8.18 (s, 1H), 8.05 (d, $J = 8.2$ Hz, 1H), 7.80 (d, $J = 7.8$ Hz, 1H), 7.65 (t, $J = 7.9$ Hz, 1H). ^{13}C NMR (151 MHz, CDCl_3) δ : 134.6, 134.5, 133.8, 133.5, 131.6, 130.6, 129.9, 117.7, 113.5. MS (EI) m/z : 251.9 $[\text{M}-1]^+$, 253.9 $[\text{M}+1]^+$.

(Z)-4-(2-bromo-2-nitrovinyl) benzonitrile (**HS28**)

Yield 67%. Yellow solid. M.p.: 148 – 150 °C. ^1H NMR (600 MHz, CDCl_3) δ : 8.62 (s, 1H), 7.96 (d, $J = 8.2$ Hz, 2H), 7.79 (d, $J = 8.3$ Hz, 2H). ^{13}C NMR (151 MHz, CDCl_3) δ : 134.6, 134.2, 132.5, 130.9, 117.9, 114.8. MS (EI) m/z : 251.9 $[\text{M}-1]^+$, 253.9 $[\text{M}+1]^+$.

(Z)-1-(2-bromo-2-nitrovinyl)-3-fluorobenzene (**HS29**)

Yield 64%. Yellow solid. M.p.: 41 – 42 °C. ^1H NMR (600 MHz, CDCl_3) δ : 8.58 (s, 1H), 7.67 (d, $J = 9.6$ Hz, 1H), 7.60 (d, $J = 7.8$ Hz, 1H), 7.48 (q, $J = 7.8$ Hz, 1H), 7.23 (t, $J = 8.2$ Hz, 1H). ^{13}C NMR (151 MHz, CDCl_3) δ : 163.3, 161.7, 135.1, 132.1, 130.6, 129.2, 127.2, 118.8, 116.8, 94.8. MS (EI) m/z : 244.9 $[\text{M}-1]^+$, 246.9 $[\text{M}+1]^+$.

(Z)-1-(2-bromo-2-nitrovinyl)-4-fluorobenzene (**HS30**)

Yield 68%. Yellow solid. M.p.: 52 – 53 °C. ^1H NMR (600 MHz, CDCl_3) δ : 8.63 (s, 1H), 7.94 (dd, $J = 8.7, 5.4$ Hz, 2H), 7.20 (t, $J = 8.6$ Hz, 2H). ^{13}C NMR (151 MHz, CDCl_3) δ : 165.4, 163.7, 135.3, 133.4, 127.8, 126.3, 116.4. MS (EI) m/z : 244.8 $[\text{M}-1]^+$, 246.9 $[\text{M}+1]^+$. HRMS (ESI) m/z calcd $\text{C}_8\text{H}_5\text{NO}_2\text{FBr}$ $[\text{M} + \text{CH}_3\text{O}]^+$ 275.9677, found 275.9676.

(Z)-1-chloro-3-(2-chloro-2-nitrovinyl) benzene (**HS31**)

Yield 79%. Yellow solid. M.p.: 45 – 46 °C. ^1H NMR (600 MHz, CDCl_3) δ : 8.28 (s, 1H), 7.83 (s, 1H), 7.70 (d, $J = 7.6$ Hz, 1H), 7.48 (d, $J = 8.1$ Hz, 1H), 7.44 (t, $J = 7.8$ Hz, 1H). ^{13}C NMR (151 MHz, CDCl_3) δ : 133.4, 129.9, 126.6, 126.1, 125.3, 125.1, 124.9, 124.2. MS (EI) m/z : 216.9 $[\text{M}]^+$.

(Z)-1-chloro-4-(2-chloro-2-nitrovinyl) benzene (HS32)

Yield 80%. Yellow solid. M.p.: 58 – 60 °C. ¹H NMR (600 MHz, CDCl₃) δ: 8.38 (s, 1H), 7.85 (d, *J* = 8.1 Hz, 2H), 7.52 (d, *J* = 8.0 Hz, 2H). ¹³C NMR (151 MHz, CDCl₃) δ: 137.7, 137.5, 131.9, 129.9, 129.1, 127.6. MS (EI) *m/z*: 216.9 [M]⁺.

(Z)-3-(2-chloro-2-nitrovinyl) benzonitrile (HS33)

Yield 72%. Yellow solid. M.p.: 106 – 108 °C. ¹H NMR (600 MHz, CDCl₃) δ: 8.36 (s, 1H), 8.16 (s, 1H), 8.05 (d, *J* = 7.9 Hz, 1H), 7.81 (d, *J* = 7.7 Hz, 1H), 7.66 (t, *J* = 7.9 Hz, 1H). ¹³C NMR (151 MHz, CDCl₃) δ: 134.4, 129.7, 129.4, 128.6, 125.8, 124.9, 123.8, 112.5, 108.5. MS (EI) *m/z*: 208.1 [M]⁺. MS (EI) *m/z*: 208.0 [M]⁺. HRMS (ESI) *m/z* calcd C₉H₅N₂O₂Cl [M + CH₃O]⁺ 239.0229, found 239.0236.

(Z)-4-(2-chloro-2-nitrovinyl) benzonitrile (HS34)

Yield 73%. Yellow solid. M.p.: 138 – 140 °C. ¹H NMR (600 MHz, CDCl₃) δ: 8.37 (s, 1H), 7.95 (d, *J* = 8.2 Hz, 2H), 7.80 (d, *J* = 8.2 Hz, 2H). ¹³C NMR (151 MHz, CDCl₃) δ: 134.8, 128.8, 127.5, 126.0, 124.1, 112.7, 109.7. MS (EI) *m/z*: 208.0 [M]⁺. HRMS (ESI) *m/z* calcd C₉H₅N₂O₂Cl [M + CH₃O]⁺ 239.0229, found 239.0236.

(Z)-1-(2-chloro-2-nitrovinyl)-3-nitrobenzene (HS35)

Yield 67%. Yellow solid. M.p.: 111 – 112 °C. ¹H NMR (600 MHz, CDCl₃) δ: 8.76 (s, 1H), 8.43 (s, 1H), 8.38 (d, *J* = 8.2 Hz, 1H), 8.15 (d, *J* = 7.6 Hz, 1H), 7.78 – 7.70 (m, 1H). ¹³C NMR (151 MHz, CDCl₃) δ: 136.0, 135.8, 133.3, 130.9, 129.8, 128.4, 125.6, 124.8. MS (EI) *m/z*: 217.1 [M]⁺. HRMS (ESI) *m/z* calcd C₈H₅N₂O₄Cl [M + CH₃O]⁺ 259.0127, found 259.0127.

(Z)-1-(2-chloro-2-nitrovinyl)-4-nitrobenzene (HS36)

Yield 68%. Yellow solid. M.p.: 98 – 100 °C. ¹H NMR (600 MHz, CDCl₃) δ: 8.42 (s, 1H), 8.36 (d, *J* = 8.7 Hz, 2H), 8.02 (d, *J* = 8.7 Hz, 2H). ¹³C NMR (151 MHz, CDCl₃) δ: 148.5, 135.3, 133.4, 131.2, 128.4, 123.7. MS (EI) *m/z*: 217.1 [M]⁺.

4.2 FBPase inhibition assays

The protein expression and purity, and FBPase inhibition assays were performed for detection compounds inhibitory activities as previously described[39].

4.3 Gluconeogenesis inhibition in mouse hepatocytes.

Primary hepatocytes were isolated from C57BLKS mice that were fasted overnight as described previously[40, 41], and then seeded in 24-well plates (2×10^5 cells per cell) in DMEM (Invitrogen™) containing 1 g/L glucose and 10% fetal bovine serum (FBS). After a 4-h attachment period, the cells were incubated overnight after being added fresh medium. Then the medium was replaced with 500 μ L of DMEM without glucose and phenol red, but supplemented with 20 mM sodium lactate and 2 mM sodium pyruvate as well as the test compounds at the desired concentrations in three parallel wells. After 4 h of incubation, 50 μ L of culture supernatant was collected, and the glucose concentration was determined using a colorimetric glucose assay kit (Fudan-Zhang-jiang™, Shanghai, China).

4.4 Molecular docking

The crystal structure of FBPase (PDB: 4H46) complexed with F6P and AMP was downloaded from the RSCB Protein Data Bank. Compound **HS13** and **HS36** were built and optimized in SYBYL 1.3. Then, **HS13** and **HS36** were docked into the C128 site of FBPase by using the covalent module of Autodock[42]. The docking process used the default parameters except the “generate diverse solution” option was chosen to enhance the variety of docked conformations.

Author information

Corresponding author

To whom correspondence should be addressed. Phone: +86-27-67862022. Fax: +86-27-67862022. E-mails : yanjvfen@163.com; E-mails: renyl@mail.ccnu.edu.cn.

Author Contributions

The manuscript was written through contributions of all authors. All authors have given approval to the final version of the manuscript. # These authors contributed equally.

Notes

The authors declare no competing financial interest.

Acknowledgments

This work was supported by the National Key R&D Program of China (No. 2017YFE0118200), the Anhui Key Research and Development Program (No. 201904b11020025), the Natural Science Foundation of Anhui Province, China (No. 1908085MB35), the Natural Science Foundation for the Higher Education Institutions of Anhui Province of China (No. KJ2018A0040), the China-Hungary Cooperation Committee Regular Meeting Exchange Project (No. 2018-II-2), the China-Ukraine Cooperation Committee Regular Meeting Exchange Project (No. CU03-04), the Open Project Program of Key Laboratory of Pesticide & Chemical Biology (CCNU), Ministry of Education (No. 201801A02). We would like to thank professor Wenjing Xiao from central China normal university for providing us with compound **HS23**.

ABBREVIATIONS

FBPase, fructose-1,6-bisphosphatase; FBP, fructose-1,6-biphosphate; F6P, fructose-6-biphosphate; IC₅₀, half maximal inhibitory concentration; T2DM, Type 2 diabetes mellitus; SAR, structure–activity relationship; GNG, gluconeogenesis; AMP, adenosine monophosphate; DMEM, Dulbecco's modified Eagle's medium.

REFERENCES

- [1] W. Yang, J. Lu, J. Weng, W. Jia, L. Ji, J. Xiao, Z. Shan, J. Liu, H. Tian, Q. Ji, D. Zhu, J. Ge, L. Lin, L. Chen, X. Guo, Z. Zhao, Q. Li, Z. Zhou, G. Shan, J. He, D. China National, G. Metabolic Disorders Study, Prevalence of diabetes among men and women in China, *N. Engl. J. Med.*, 362 (2010) 1090-1101.
- [2] S.E. Kahn, M.E. Cooper, S. Del Prato, Pathophysiology and treatment of type 2 diabetes: perspectives on the past, present, and future, *The Lancet*, 383 (2014) 1068-1083.
- [3] S. Chatterjee, K. Khunti, M.J. Davies, Type 2 diabetes, *The Lancet*, 389 (2017) 2239-2251.
- [4] A. Wagman, J. Nuss, Current Therapies and Emerging Targets for the Treatment of Diabetes, *Curr. Pharm. Des.*, 7 (2001) 417-450.
- [5] D.E. Moller, New drug targets for type 2 diabetes and the metabolic syndrome, *Nature*, 414 (2001) 821-827.
- [6] N. Kerru, A. Singh-Pillay, P. Awolade, P. Singh, Current anti-diabetic agents and their molecular targets: A review, *Eur. J. Med. Chem.*, 152 (2018) 436-488.
- [7] L.K.J. Stadler, I.S. Farooqi, A New Drug Target for Type 2 Diabetes, *Cell*, 170 (2017) 12-14.
- [8] A.K. Madiraju, D.M. Erion, Y. Rahimi, X.M. Zhang, D.T. Braddock, R.A. Albright, B.J. Prigaro, J.L. Wood, S. Bhanot, M.J. MacDonald, M.J. Jurczak, J.P. Camporez, H.Y. Lee, G.W. Cline, V.T. Samuel, R.G. Kibbey, G.I. Shulman, Metformin suppresses gluconeogenesis by inhibiting mitochondrial glycerophosphate dehydrogenase, *Nature*, 510 (2014) 542-546.
- [9] R.A. Miller, Q. Chu, J. Xie, M. Foretz, B. Viollet, M.J. Birnbaum, Biguanides suppress hepatic glucagon signalling by decreasing production of cyclic AMP, *Nature*, 494 (2013) 256-260.
- [10] B.R. Landau, J. Wahren, V. Chandramouli, W.C. Schumann, K. Ekberg, S.C. Kalhan, Contributions of gluconeogenesis to glucose production in the fasted state, *J. Clin. Invest.*, 98 (1996) 378-385.

- [11] P.D. van Poelje, S.C. Potter, V.C. Chandramouli, B.R. Landau, Q. Dang, M.D. Erion, Inhibition of fructose 1,6-bisphosphatase reduces excessive endogenous glucose production and attenuates hyperglycemia in Zucker diabetic fatty rats, *Diabetes*, 55 (2006) 1747-1754.
- [12] A.K. Rines, K. Sharabi, C.D.J. Tavares, P. Puigserver, Targeting hepatic glucose metabolism in the treatment of type 2 diabetes, *Nat. Rev. Drug Discov.* 15 (2016) 786-804.
- [13] Q. Dang, S.R. Kasibhatla, K.R. Reddy, T. Jiang, M.R. Reddy, S.C. Potter, J.M. Fujitaki, P.D. van Poelje, J. Huang, W.N. Lipscomb, M.D. Erion, Discovery of potent and specific fructose-1,6-bisphosphatase inhibitors and a series of orally-bioavailable phosphoramidase-sensitive prodrugs for the treatment of type 2 diabetes, *J. Am. Chem. Soc.*, 129 (2007) 15491-15502.
- [14] H. Ke, Thorpe, C. M., Seaton, B. A., Lipscomb, W. N., & Marcus, F., Structure refinement of fructose-1,6-bisphosphatase and its fructose 2,6-bisphosphate complex at 2.8 Å resolution. , *J. Mol. Biol.*, 212 (1990) 513-539.
- [15] Y. Gao, L. Shen, R.B. Honzatko, Central cavity of fructose-1,6-bisphosphatase and the evolution of AMP/fructose 2,6-bisphosphate synergism in eukaryotic organisms, *J. Biol. Chem.*, 289 (2014) 8450-8461.
- [16] J.K. Hines, X. Chen, J.C. Nix, H.J. Fromm, R.B. Honzatko, Structures of mammalian and bacterial fructose-1,6-bisphosphatase reveal the basis for synergism in AMP/fructose 2,6-bisphosphate inhibition, *J. Biol. Chem.*, 282 (2007) 36121-36131.
- [17] M. Gidh-Jain, Y. Zhang, P. van Poelje, J. Liang, S. Huang, J. Kim, J. Elliott, M. Erion, The allosteric site of human liver fructose-1,6-bisphosphatase. Analysis of six AMP site mutants based on the crystal structure, *J. Biol. Chem.*, 269 (1994) 27732-27738.
- [18] R.W. Hunter, C.C. Hughey, L. Lantier, E.I. Sundelin, M. Pegg, E. Zeqiraj, F. Sicheri, N. Jessen, D.H. Wasserman, K. Sakamoto, Metformin reduces liver glucose production by inhibition of fructose-1-6-bisphosphatase, *Nat. Med.*, 24 (2018) 1395-1406.
- [19] M. Kebede, J. Favaloro, J.E. Gunton, D.R. Laybutt, M. Shaw, N. Wong, B.C. Fam,

K. Aston-Mourney, C. Rantzau, A. Zulli, J. Proietto, S. Andrikopoulos, Fructose-1,6-Bisphosphatase Overexpression in Pancreatic β -Cells Results in Reduced Insulin Secretion: A New Mechanism for Fat-Induced Impairment of β -Cell Function, *Diabetes*, 57 (2008) 1887-1895.

[20] S.W. Wright, D.L. Hageman, L.D. McClure, A.A. Carlo, J.L. Treadway, A.M. Mathiowetz, J.M. Withka, P.H. Bauer, Allosteric inhibition of fructose-1,6-bisphosphatase by anilinoquinazolines, *Bioorg. Med. Chem. Lett.*, 11 (2001) 17-21.

[21] C. Lai, R.J. Gum, M. Daly, E.H. Fry, C. Hutchins, C. Abad-Zapatero, T.W. von Geldern, Benzoxazole benzenesulfonamides as allosteric inhibitors of fructose-1,6-bisphosphatase, *Bioorg. Med. Chem. Lett.*, 16 (2006) 1807-1810.

[22] M.D. Erion, Q. Dang, M.R. Reddy, S.R. Kasibhatla, J. Huang, W.N. Lipscomb, P.D. van Poelje, Structure-guided design of AMP mimics that inhibit fructose-1,6-bisphosphatase with high affinity and specificity, *J. Am. Chem. Soc.*, 129 (2007) 15480-15490.

[23] Q. Dang, S.R. Kasibhatla, T. Jiang, K. Fan, Y. Liu, F. Taplin, W. Schulz, D.K. Cashion, K.R. Reddy, P.D. van Poelje, J.M. Fujitaki, S.C. Potter, M.D. Erion, Discovery of phosphonic diamide prodrugs and their use for the oral delivery of a series of fructose 1,6-bisphosphatase inhibitors, *J. Med. Chem.*, 51 (2008) 4331-4339.

[24] P. Hebeisen, B. Kuhn, P. Kohler, M. Gubler, W. Huber, E. Kitas, B. Schott, J. Benz, C. Joseph, A. Ruf, Allosteric FBPase inhibitors gain 10(5) times in potency when simultaneously binding two neighboring AMP sites, *Bioorg. Med. Chem. Lett.*, 18 (2008) 4708-4712.

[25] S. Heng, K.R. Gryncel, E.R. Kantrowitz, A library of novel allosteric inhibitors against fructose 1,6-bisphosphatase, *Bioorg. Med. Chem.*, 17 (2009) 3916-3922.

[26] A. Rudnitskaya, K. Huynh, B. Torok, K. Stieglitz, Novel heteroaromatic organofluorine inhibitors of fructose-1,6-bisphosphatase, *J. Med. Chem.*, 52 (2009) 878-882.

[27] T. Tsukada, M. Takahashi, T. Takemoto, O. Kanno, T. Yamane, S. Kawamura, T. Nishi, Synthesis, SAR, and X-ray structure of tricyclic compounds as potent FBPase inhibitors, *Bioorg. Med. Chem. Lett.*, 19 (2009) 5909-5912.

- [28] E. Kitas, P. Mohr, B. Kuhn, P. Hebeisen, H.P. Wessel, W. Haap, A. Ruf, J. Benz, C. Joseph, W. Huber, R.A. Sanchez, A. Paehler, A. Benardeau, M. Gubler, B. Schott, E. Tozzo, Sulfonylureido thiazoles as fructose-1,6-bisphosphatase inhibitors for the treatment of type-2 diabetes, *Bioorg. Med. Chem. Lett.*, 20 (2010) 594-599.
- [29] P. Yi, Y.T. Di, W. Liu, X.J. Hao, Y. Ming, D.S. Huang, J. Yang, Z.Z. Yi, Z.J. Li, R.D. Yang, J.C. Zhang, Protein-based alignment in 3D-QSAR of FBPase inhibitors, *Eur. J. Med. Chem.*, 46 (2011) 885-892.
- [30] R.F. Tayyem, H.M. Zalloum, M.R. Elmaghrabi, A.M. Yousef, M.S. Mubarak, Ligand-based designing, in silico screening, and biological evaluation of new potent fructose-1,6-bisphosphatase (FBPase) inhibitors, *Eur. J. Med. Chem.*, 56 (2012) 70-95.
- [31] J. Bie, S. Liu, Z. Li, Y. Mu, B. Xu, Z. Shen, Discovery of novel indole derivatives as allosteric inhibitors of fructose-1,6-bisphosphatase, *Eur. J. Med. Chem.*, 90 (2015) 394-405.
- [32] B.R. Liao, H.B. He, L.L. Yang, L.X. Gao, L. Chang, J. Tang, J.Y. Li, J. Li, F. Yang, Synthesis and structure-activity relationship of non-phosphorus-based fructose-1,6-bisphosphatase inhibitors: 2,5-Diphenyl-1,3,4-oxadiazoles, *Eur. J. Med. Chem.*, 83 (2014) 15-25.
- [33] M.D. Erion, P.D. van Poelje, Q. Dang, S.R. Kasibhatla, S.C. Potter, M.R. Reddy, K.R. Reddy, T. Jiang, W.N. Lipscomb, MB06322 (CS-917): A potent and selective inhibitor of fructose 1,6-bisphosphatase for controlling gluconeogenesis in type 2 diabetes, *Proc. Natl. Acad. Sci. U S A*, 102 (2005) 7970-7975.
- [34] J. Singh, R.C. Petter, T.A. Baillie, A. Whitty, The resurgence of covalent drugs, *Nat. Rev. Drug Discov.*, 10 (2011) 307-317.
- [35] T.A. Baillie, Targeted Covalent Inhibitors for Drug Design, *Angew. Chem. Int. Ed. Engl.*, 55 (2016) 13408-13421.
- [36] R. Lonsdale, R.A. Ward, Structure-based design of targeted covalent inhibitors, *Chem. Soc. Rev.*, 47 (2018) 3816-3830.
- [37] P. Chatterjee, W.M. Botello-Smith, H. Zhang, L. Qian, A. Alsamarah, D. Kent, J.J. Lacroix, M. Baudry, Y. Luo, Can Relative Binding Free Energy Predict Selectivity of Reversible Covalent Inhibitors?, *J. Am. Chem. Soc.*, (2017).

- [38] S. De Cesco, J. Kurian, C. Dufresne, A.K. Mittermaier, N. Moitessier, Covalent inhibitors design and discovery, *Eur. J. Med. Chem.*, 138 (2017) 96-114.
- [39] Y. Huang, L. Wei, X. Han, H. Chen, Y. Ren, Y. Xu, R. Song, L. Rao, C. Su, C. Peng, L. Feng, J. Wan, Discovery of novel allosteric site and covalent inhibitors of FBPase with potent hypoglycemic effects, *Eur. J. Med. Chem.*, 184 (2019) 111749.
- [40] J.C. Yoon, P. Puigserver, G. Chen, J. Donovan, Z. Wu, J. Rhee, G. Adelman, J. Stafford, C.R. Kahn, D.K. Granner, Control of hepatic gluconeogenesis through the transcriptional coactivator PGC-1, *Nature*, 413 (2001) 131-138.
- [41] S.-H. Koo, H.C. Towle, Glucose Regulation of Mouse S14 Gene Expression in Hepatocytes INVOLVEMENT OF A NOVEL TRANSCRIPTION FACTOR COMPLEX, *J. Biol. Chem.*, 275 (2000) 5200-5207.
- [42] G.M. Morris, H. Ruth, L. William, M.F. Sanner, R.K. Belew, D.S. Goodsell, A.J. Olson, AutoDock4 and AutoDockTools4: Automated docking with selective receptor flexibility, *J. Comput. Chem.*, 30 (2010) 2785-2791.

Conflict of interest

The authors declared that they have no conflicts of interest to this work.

We declare that we do not have any commercial or associative interest that represents a conflict of interest in connection with the work submitted.

